Monocyte accumulation in mouse atherogenesis is progressive and proportional to extent of disease

Filip K. Swirski*†‡, Mikael J. Pittet*‡, Moritz F. Kircher*, Elena Aikawa*, Farouc A. Jaffer*, Peter Libby†, and Ralph Weissleder*§

*Center for Molecular Imaging Research and Donald W. Reynolds Cardiovascular Clinical Research Center on Atherosclerosis at Harvard Medical School, Massachusetts General Hospital and Harvard Medical School, CNY 149, Charlestown, MA 02129; and †Cardiovascular Division, Department of Medicine and Donald W. Reynolds Cardiovascular Clinical Research Center on Atherosclerosis at Harvard Medical School, Brigham and Women's Hospital and Harvard Medical School, 75 Francis Street, Boston, MA 02115

Communicated by Daniel Steinberg, University of California at San Diego School of Medicine, La Jolla, CA, May 26, 2006 (received for review January 2, 2006)

Monocytes participate importantly in the pathogenesis of atherosclerosis, but their spatial and temporal recruitment from circulation remains uncertain. This study tests the hypothesis that monocyte accumulation in atheroma correlates with the extent of disease by using a sensitive and simple quantitative assay that allows tracking of highly enriched populations of blood monocytes. A two-step isolation method yielded viable and functionally intact highly enriched peripheral blood monocyte populations (>90%). Recipient mice received syngeneic monocytes labeled in two ways: by transgenically expressing EGFP or with a radioactive tracer [^{111}In]oxine. After 5 days, more labeled cells accumulated in the aorta, principally the aortic root and ascending aorta, of 10-wk-old ApoE$^{-/-}$ compared with 10-wk-old C57BL/6 mice (223 ± 3 vs. 87 ± 22 cells per aorta). Considerably more monocytes accumulated in 20-wk-old ApoE$^{-/-}$ mice on either chow (314 ± 41 cells) or high-cholesterol diet (395 ± 53 cells). Fifty-week-old ApoE$^{-/-}$ mice accumulated even more monocytes in the aortic root, ascending aorta, and thoracic aorta after both chow (503 ± 67 cells) or high-cholesterol diet (648 ± 81 cells). Labeled monocyte content in the aorta consistently correlated with lesion surface area. These data indicate that monocytes accumulate continuously during atheroma formation, accumulation increases in proportion to lesion size, and recruitment is augmented with hypercholesterolemia. These results provide insights into mechanisms of atherogenesis and have implications for the duration of therapies directed at leukocyte recruitment.

atherosclerosis | imaging | leukocyte

The progression of atherosclerotic plaques involves the accumulation of cholesterol in the arterial wall, inflammation, leukocyte recruitment, and development of fibrotic lesions (1, 2). Monocyte accumulation in the intima characterizes fatty streaks, the earliest visible lesion of human and experimental atherosclerosis. In the intima, monocytes differentiate into macrophages, ingest modified lipoproteins via scavenger receptors, and secrete inflammatory mediators that can stimulate smooth muscle cell migration and proliferation. Lipid-rich macrophages, i.e., foam cells, become key constituents of the plaque's lipid core.

Despite the crucial role of macrophages in atherogenesis (3, 4), the dynamics of this accumulation remain poorly understood. For example, whether monocyte recruitment to atherosclerotic lesions occurs continuously or peaks and wanes at specific stages during the natural history of a lesion, as occurs in T cell recruitment, remains undetermined (5–7). Lesional leukokinetics have important implications for the prevention and treatment of atherosclerosis, because they could identify optimal times to modulate cellular recruitment. However, murine monocytes occur in relatively small numbers in peripheral blood and do not express a known unique marker. Their isolation, therefore, presents a challenge and accounts for the current paucity of kinetic data on pure monocyte populations in atherosclerosis.

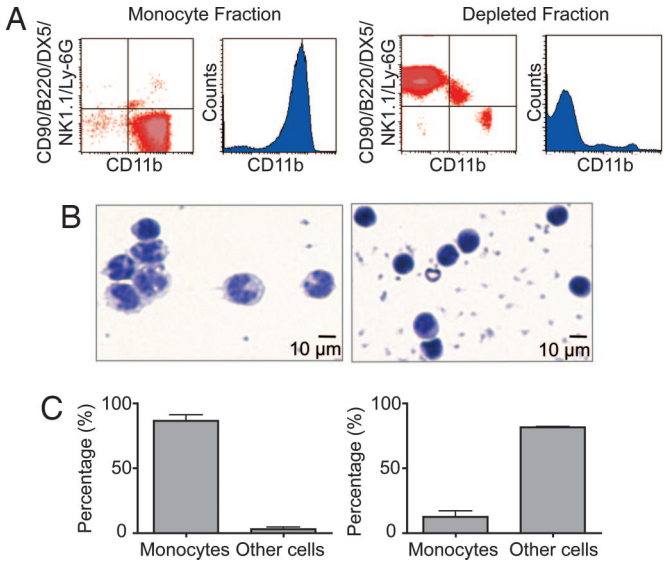

Fig. 1. Monocyte isolation. (*A*) The monocyte fraction (*Left*) and the depleted fraction (*Right*) were stained with anti-CD11b, CD90, B220, DX5, NK1.1, and Ly-6G mAbs. (*B*) Representative cytospin preparations of the cell fractions. (*C*) Proportion of monocytes and other cells based on morphology and calculated by counting 10 high-power fields. Three independent experiments yielded similar results.

This study used a two-step method for purifying mouse peripheral blood monocytes to high purity while keeping them viable, functional, and in a resting state. To test the hypothesis that isolated monocytes indeed accumulate in atherosclerotic lesions, we applied different tagging strategies to follow donor cells in recipient-animal cohorts. In some cohorts, lesion deposition of adoptively transferred EGFP-expressing monocytes was assessed by immunohistochemistry. Another approach used monocytes labeled with the FDA-approved radioactive tracer [^{111}In]oxine and tracked these adoptively transferred cells by biodistribution analysis and by their spatial distribution within aortas, followed by correlation with lesion burden. The observation that increased lesion size correlates directly with increased leukocyte recruitment has implications for the prevention and treatment of disease. Additionally, therapies that target

Conflict of interest statement: No conflicts declared.

Abbreviations: NK, natural killer; ORO, Oil red O.

‡F.K.S. and M.J.P. contributed equally to this work.

§To whom correspondence should be addressed at: Center for Molecular Imaging Research, Massachusetts General Hospital, 13th Street, Building 149, Room 5403, Charlestown, MA 02129. E-mail: weissleder@helix.mgh.harvard.edu.

www.pnas.org/cgi/doi/10.1073/pnas.0604260103

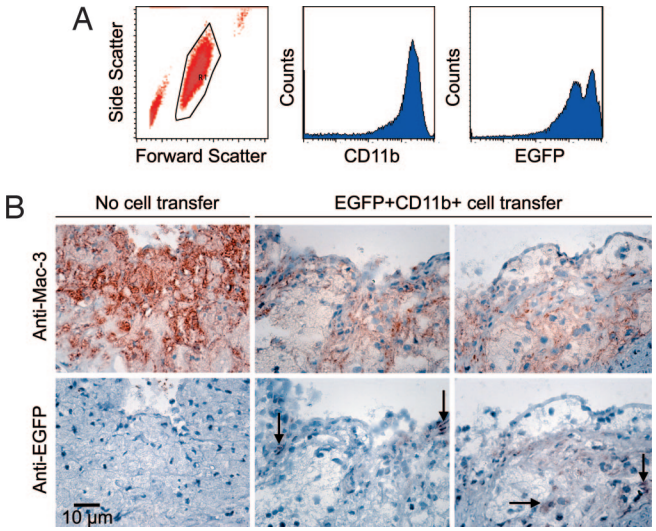

Fig. 2. Detection of monocytes in aortic lesions. (*A*) Assessment of purity of isolated monocytes from EGFP-expressing mice stained with anti CD11b. (*B*) Monocytes were injected i.v. into 20-wk-old ApoE$^{-/-}$ mice on a high-cholesterol diet. Five days after injection, the aortas were excised, and immunohistochemistry was conducted with Abs against Mac-3 and EGFP. High-power fields of the lesion area at the root from mice that did not receive EGFP^{+} cells (*Left*) and from mice that received EGFP^{+} cells (*Center* and *Right* representing different sections) stained with anti-Mac-3 (*Upper*) and anti-EGFP (*Lower*). Data are representative of three independent experiments.

monocyte chemoattractant and adhesion molecules may require long-term administration to durably suppress monocyte recruitment and consequent atherogenesis.

Results

Isolation and Purification of Functional Monocytes. To isolate circulating monocytes with sufficiently high purity, we first optimized a protocol adapted from several studies (8–10). Peripheral blood from C57BL/6 mice was obtained by cardiac puncture and first subjected to density-gradient centrifugation (enrichment of mononuclear cells, depletion of granulocytes and erythrocytes) and then to magnetic cell sorting to deplete T cells, B cells, natural killer (NK) cells, and any contaminating erythrocytes that remained after the first step. Phenotypic and morphologic homogeneity of monocytes in a sample of the isolated cells was routinely assessed. The monocyte fraction contained a population of which nearly all cells (90.8 ± 3.0%) expressed CD11b, an integrin expressed on myeloid cells, activated T cells, B cells, NK cells, and granulocytes. Of these, nearly all cells (>97%) were negative for CD90 (T cells), B220 (B cells), DX5 and NK1.1 (NK cells), and Ly-6G (granulocytes) (Fig. 1*A*). Correspondingly, the fraction containing the magnetically depleted cells contained mostly lymphocytes (92.2 ± 4.9%) and only a small fraction of monocytes (5.8 ± 1.8%). Morphological assessment of the isolated monocyte fractions revealed variably sized cells with a horseshoe- or kidney-shaped nucleus, variable nucleus-to-cytoplasm ratio, and vacuoles, all typical of monocytes (Fig. 1 *B* and *C*). The isolation protocol did not activate the cells based on phenotypic analysis because (*i*) CD11b and CD62L expression before and after isolation were unchanged and (*ii*) purified monocytes did not up-regulate markers of activated monocytes/mature macrophages or dendritic cells, such as F4/80 and MHC-II (data not shown). The cytospins showed no platelet adherence to monocytes, a phenomenon that may occur from platelet activation during initial centrifugation. This is an important result, because activated platelets themselves participate in atherogenesis (11, 12).

Adoptively Transferred Monocytes Have Affinity for Atherosclerotic Lesions. To localize labeled cells in atherosclerotic lesions, isolated EGFP^{+} CD11b^{+} cells (1×10^{6}) were first injected into 20-wk-old ApoE$^{-/-}$ mice on a Western high-cholesterol diet (Fig. 2*A*). In animals that received EGFP^{+} CD11b^{+} cells systemically, the intima of atherosclerotic lesions showed focal EGFP^{+} immunohistochemical signal (Fig. 2*B*, arrows). Animals that did not receive cells showed no such signal. EGFP-expressing cells colocalized with sites of highest Mac-3 signal, a marker of mature macrophages, suggesting migration of EGFP^{+} cells to macrophage-rich lesions. Despite analysis of adjacent

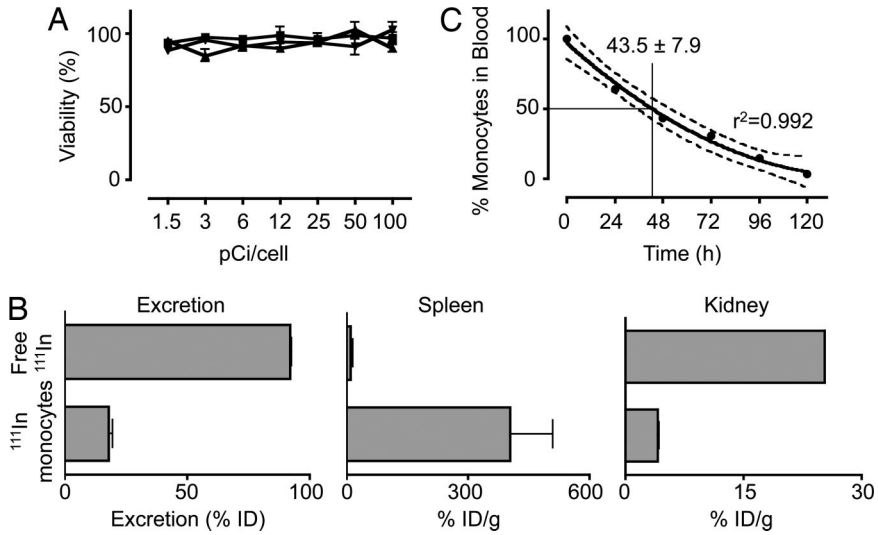

Fig. 3. Labeling, excretion, and organ distribution of ^{111}In species. (*A*) MTS assay of monocytes labeled with increasing doses of decayed [^{111}In]oxine (squares), [^{111}In]oxine (triangles), or [^{111}In]chloride (inverted triangles). (*B*) Biodistribution of [^{111}In]oxine-labeled monocytes compared with biodistribution of ^{111}In alone 5 d after i.v. injection. (*C*) Retention of monocytes in the circulation. [^{111}In]oxine-labeled monocytes were injected i.v., and radioactivity was measured in blood withdrawals. Biodistribution measured immediately after injection was normalized to 100%. The range of monocyte blood half-life is calculated from a 95% confidence interval, as determined from a polynomial second-order fit. (n = 2–8; mean ± SEM).

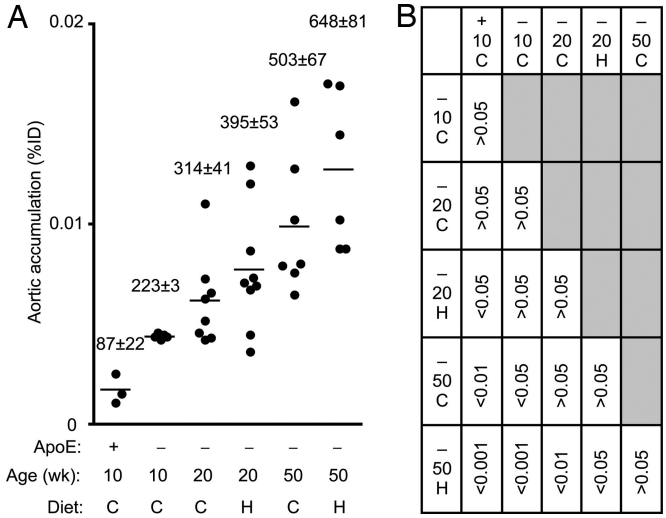

Fig. 4. Accumulation of monocytes in the aorta. [^{111}In]oxine-labeled monocytes were injected into WT or ApoE$^{-/-}$ mice (ApoE: + or −, respectively) of different age [Age (wk): 10, 20, or 50] and on either chow or high-cholesterol diets (diet C or H, respectively). Five days after injection, aortas were excised. (*A*) Percent injected dose per aorta. The data above the graph represent mean monocyte number ± SEM for each group. (*B*) Statistics (*P* value) for each group were calculated by using one-way ANOVA with Tukey's multiple-comparison test.

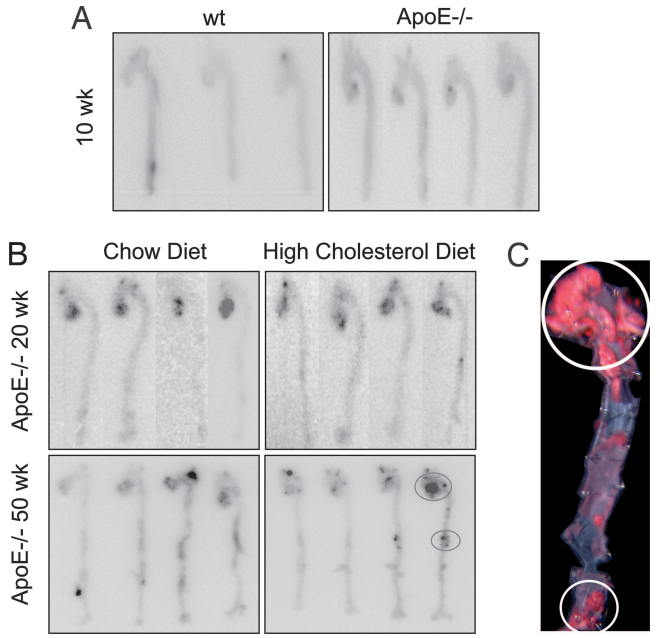

Fig. 5. Localization of monocytes in aorta. [^{111}In]oxine-labeled monocytes were injected into 10-wk-old WT (*A Left*) or ApoE$^{-/-}$ (*A Right*) mice and 20-wk-old (*B Upper*) and 50-wk-old (*B Lower*) ApoE$^{-/-}$ mice on chow (*B Left*) or high-cholesterol (*B Right*) diet. Five days after injection, aortas were excised, exposed to imaging plates, and subsequently read out by a PhosphorImager. Representative aortas are shown. (*C*) ORO staining of excised aorta from a 50-wk-old mouse on a high-cholesterol diet. Highest ORO staining typically mapped to highest radioactivity (circles).

sections, we were unable to conclude whether EGFP^{+} cells acquired expression of Mac-3.

Quantification of Recruitment of Isotope-Labeled Cells to Atheroma. We next sought to characterize [^{111}In]oxine-labeled monocyte accumulation in the aortas of mice of different ages on different diets. Initially, we found that monocyte viability was >90% for all experiments within 24 h after labeling (Fig. 3*A*), and ^{111}In released from the adoptively transferred monocytes was rapidly excreted (Fig. 3*B*). Based on pilot observations, analysis was performed 5 d after injection, the time point that corresponded to >95% monocyte clearance from circulation, without losing detection of ^{111}In, which decays with a physical half-life of 2.8 d (Fig. 3*C*). The half-life of circulating blood monocytes was 43.5 ± 7.9 h (Fig. 3*C*). We also determined whether monocytes obtained from ApoE-deficient mice accumulated differently in lesions. Comparative experiments yielded no significant difference ($P = 0.23$). Because of greater accessibility and lower cost, we transferred C57BL/6-derived monocytes. Pulse experiments to quantify monocyte uptake at a given age revealed increasing accumulation in aortas during the mouse's lifespan (Fig. 4*A*). Accumulation tended to be higher in 10-wk-old ApoE$^{-/-}$ mice on chow diet (223 ± 3 cells 5 d after adoptive transfer) compared with age-matched C57BL/6 mice (87 ± 22 cells, $P > 0.05$; Fig. 4*B*). Accumulation in 20-wk-old ApoE$^{-/-}$ mice on a high-cholesterol diet was significantly greater (395 ± 53 cells) than in C57BL/6 mice but not when compared with younger or age-matched chow-fed ApoE$^{-/-}$ mice (314 ± 41 cells). At 50 wk of age, there was a statistically significant difference between high-cholesterol-fed animals (648 ± 81 cells) and all other animals except age-matched chow-fed mice (503 ± 67 cells).

Autoradiography showed consistently higher signal from labeled monocytes in lesion-rich areas. The aortic root of ApoE$^{-/-}$ mice, but not WT C57BL/6 mice, had regions of enhanced radioactivity in 10-wk-old mice (Fig. 5*A*). In 20-wk-old mice, high-activity regions predominated in the root and ascending aorta (Fig. 5*B*), whereas, in 50-wk-old mice, discrete regions localized in the root and along the entire aorta, especially the thoracic aorta; younger mice did not otherwise show areas of increased activity (Fig. 5*B*). A representative lipid stain for visualization of aortic lesion in a 50-wk-old ApoE$^{-/-}$ mouse on a high-cholesterol diet is shown in Fig. 5*C*.

Correlation of Signal to Serum Cholesterol Levels and Lesion Area. We next determined whether aortic monocyte accumulation correlated with serum cholesterol levels and with lesion area as quantified by Oil red O (ORO) staining. Serum cholesterol levels correlate positively with lesion burden (Fig. 6*A*), as reported (13, 14). We further compared serum cholesterol levels in mice of different ages and on different diets and determined, as expected, higher levels in animals on a high-fat diet but similar in 20- and 50-wk-old mice on the same diet (Fig. 6*B*). Additionally, separate studies of aortic accumulation and serum cholesterol levels in 20- (Fig. 6*C*) and 50-wk-old (Fig. 6*D*) mice indicated a positive correlation between these two parameters in older animals. To test whether greater accumulation resulted exclusively from a larger lesion surface area or whether greater accumulation also related to a change in monocyte accumulation per unit area, we correlated the percent lesion area with monocyte accumulation (Fig. 6*E*). Because linear regression showed a high confidence fit ($P = 0.0003$), our data strongly suggest that the rate of monocyte accumulation per lesion area remains constant.

Discussion

Studies of atherosclerotic animals have demonstrated regulation of lesion growth by a variety of inflammatory cellular and molecular components, including lymphocytes (7, 15, 16), monocytes (3, 4, 17, 18), stem cells (19), cytokines (20, 21), chemokines and chemokine receptors (22, 23), platelets (11, 12), vascular cell adhesion molecules (24), proteases (25), and costimulatory (26, 27) and intracellular signaling molecules (28). Although infor-

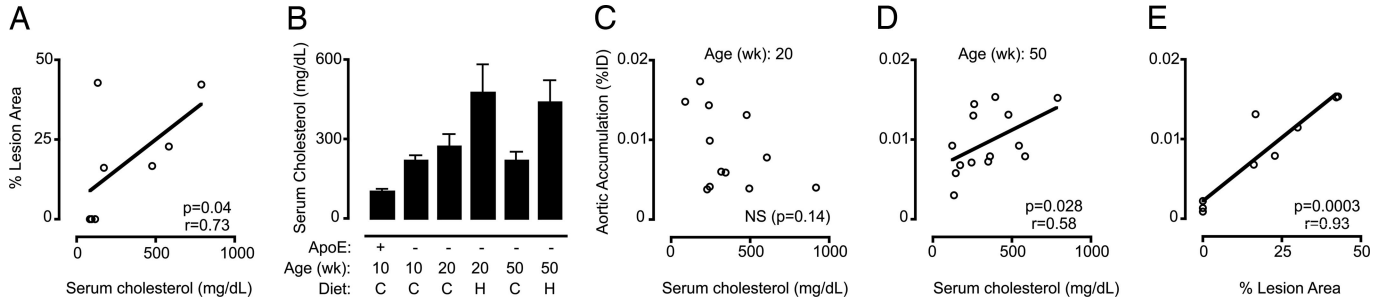

Fig. 6. Correlation of monocyte accumulation with serum cholesterol and lesion surface area. (*A*) Correlation of serum cholesterol levels with percent lesion area ($n = 8$). (*B*) Serum cholesterol levels in WT or ApoE$^{-/-}$ mice at different ages and on different diets, as identified in Fig. 4 ($n = 4$–14 per group). (*C* and *D*) Correlation between serum cholesterol and aortic accumulation in 20-wk-old (*C*) ($n = 12$) and 50-wk-old (*D*) ($n = 14$) mice, respectively. (*E*) Correlation of percent lesion area with aortic monocyte accumulation ($n = 9$). Linear regression was conducted to determine confidence of linear fit. *P* values are shown.

mative, these studies appraise static parameters, such as lesion size or cellular composition, and have provided little insight into the dynamics of cellular trafficking during lesion evolution. This gap has fostered the assumption that an increase in lesion size correlates directly with an increase in leukocyte recruitment. Experimental evaluation of this assumption by elucidating how leukocyte recruitment to the aorta correlates with and influences disease progression would have considerable interest and potentially lead to insights into the biology and therapy of atherosclerosis. This goal requires the development of sensitive, simple, precise kinetic assays that quantify cellular recruitment under various experimental conditions.

Several intravital microscopy studies described leukocyte adherence to the endothelium (18, 29, 30), implicating surface molecules (P-selectin, E-selectin, L-selectin, ICAM-1, and VCAM-1) as important in the process. The first *in vivo* studies to quantify leukocyte accumulation rather than adherence used PCR against the testis-determining gene *Sry*, present in adoptively transferred male cells (5, 31). In a seminal study, uptake of blood monocytes was examined, cells most likely to migrate across the endothelium as part of physiological atherogenesis (5). The cells transferred, however, did not express CD11b constitutively, indicating a different cell phenotype from those described here. The current study shows that highly pure and viable mouse CD11b-positive murine blood monocytes can be isolated with the use of a two-step, negative-selection method.

Assessment of accumulation in this study used immunohistochemical and isotope-based approaches in which monocytes were transferred to animals with atherosclerosis. Collectively, our studies suggest that monocytes accumulate in lesions throughout lesion growth. Although the assay allowed detection of 87 ± 22 to 648 ± 81 cells, it is possible that a fraction of the accumulated cells will, or did, migrate out of the lesions (32). That 87 ± 22 cells per aorta were detected in C57BL/6 animals may represent baseline monocyte trafficking (10) or low background levels due to residual ^{111}In. Correlational analysis indicates that the rate of accumulation per unit area remains constant.

These data contribute to the concept that atheromata actively and dynamically recruit monocytes throughout their lifetime and, thus, have important implications for therapeutic approaches that target monocyte adhesion and chemoattractant molecules. Furthermore, the described technique can be expanded to an array of other cells involved in atherosclerosis, such as immune (2) and bone marrow or blood-derived precursor cells (19).

Materials and Methods

Animals. ApoE$^{-/-}$ mice (B6.129P2-*Apoe*^{tm1Unc}), EGFP-expressing (C57BL/6-Tg(ACTB-EGFP)1Osb/J) mice, and C57BL/6 mice (6–8 wk of age) were purchased from The Jackson Laboratory. The ApoE$^{-/-}$ animals had been backcrossed to the C57BL/6 background for at least 10 generations. A total of 50 recipient and 500 donor mice were used for the studies. Mice were cared for according to the institution's animal facility guidelines. At 10 wk, a group of ApoE$^{-/-}$ animals was placed on a Western diet [21.2% fat per weight; 0.2% cholesterol (termed high-cholesterol) diet] (Harlan Teklad, Madison, WI). The remaining animals were fed a regular chow diet. All protocols were approved by the Animal Review Committee.

Monocyte Isolation. Isolation of murine peripheral blood monocytes with high purity and yield used a two-step method. Peripheral blood (0.8–1.2 ml per mouse) was drawn via cardiac puncture from donor mice anesthetized by isoflurane inhalation (Baxter Health Care, Deerfield, IL) by using a 3-ml syringe that contained 0.13 ml of anticoagulant (100 mM sodium citrate and 130 mM glucose, pH 6.5). The blood was diluted 5:1 with Hanks' balanced salt solution (HBSS) (Cellgro, Herndon, VA), overlaid on a sucrose solution (Histopaque 1083, density 1.083 g/ml; Sigma-Aldrich), and centrifuged for 45 min at 500 × *g*, at room temperature). The mononuclear cell interface was collected and washed two times in HBSS and once in magnetic cell-sorting buffer (PBS, 0.1% (wt/vol) BSA, and 0.5 mM EDTA). Cells were incubated with a mixture of antibody MicroBeads including antibodies against T cells (CD90), B cells (B220), NK cells (DX5), and erythrocytes (Ter119) according to the manufacturer's protocol (Miltenyi Biotec, Auburn, CA). The cells were then run through an LD-negative selection column. The negative (putative monocyte) fraction was collected, and cells were counted. Typically, 1 ml of blood yielded 50,000–150,000 cells in the negative fraction. To determine purity, cells were stained with phycoerythrin (PE)-CD90, PE-B220, PE-DX5, PE-NK1.1, PE-Ly-6G, and APC-CD11b (BD Biosciences). Monocytes were identified as CD11b(+) CD90(−) B220(−) DX5(−) NK1.1(−) Ly-6G (low). For morphologic characterizations, cells were spun and resuspended in PBS, and slides were prepared by cytocentrifugation (Shandon, Pittsburgh) at 10 × *g* for 2 min and stained with HEMA 3 (Biochemical Sciences, Swedesboro, NJ). Monocytes were identified as cells ranging between 10 and 30 μm in diameter, with a horseshoe- or kidney-shaped nucleus, a variable nucleus-to-cytoplasm ratio, and fine granules and vacuoli. To determine whether cell isolation led to activation, monocytes were additionally stained with MHCII, CD62L (BD Biosciences) and F4/80 (eBioscience, San Diego). The cells were deemed acceptable for further study when the monocyte purity by both flow cytometry and morphologic criteria exceeded 90%, and the cells expressed low levels of MHCII and F4/80. Typically, an isolation protocol lasted 4 h.

Immunohistochemistry. Monocytes were also isolated from EGFP-expressing mice (The Jackson Laboratory) and adoptively transferred by i.v. injection into 20-wk-old ApoE$^{-/-}$ mice. EGFP was used for its antigenic, rather than fluorescent, properties; elastin and macrophages render atheromata autofluorescent, confounding fluorescent detection. Five days after transfer, animals were killed and aortas excised, frozen in optimal cutting temperature (OCT) medium, and 5-μm cryosections prepared. Sections dried at room temperature for 20 min, were treated with 0.3% hydrogen peroxide to inhibit endogenous peroxidase activity, and incubated for 30 min in blocking solution. Adjacent sections were then incubated with primary polyclonal anti-GFP (Chemicon International, Temecula, CA) or rat anti-mouse Mac-3 antibodies (BD Biosciences) diluted in PBS supplemented with 4% of the species-respective normal serum (GFP, 1:25; Mac-3, 1:50). After washing with PBS, species-appropriate secondary antibodies were applied, followed by avidin–peroxidase complex (Vectastain ABC kit; Vector Laboratories). Slides were rinsed in PBS after each incubation step. The reaction was visualized with 3-amino-9-ethyl carbazole (AEC; Sigma-Aldrich). Sections were counterstained with Gill's hematoxylin solution (Sigma-Aldrich) and mounted. Images were captured with a digital camera (Nikon DXM1200-F) using imaging software ACT-1 version 2.63.

Monocyte Labeling and Viability. Purified monocytes were labeled with [^{111}In]oxine according to the manufacturer's protocol (Amersham Pharmacia Health Medi-Physics, Arlington Heights, IL). Briefly, cells were washed with HBSS, spun and resuspended in [^{111}In]oxine for 15 min at 37°C, pH 6.5–7.5. The cells were then washed two times with HBSS. Determination of cell viability was performed after labeling (CellTiter 95 Aqueous One Solution Cell Proliferation assay, MTS; Promega). For this procedure, purified monocytes were placed into a 96-well culture plate (5×10^5 per well) and incubated with increasing doses of [^{111}In]oxine, decayed [^{111}In]oxine (10 half-lives) or [^{111}In]chloride. After 24-h culture, absorbance was read at 490 nm with the use of a microplate reader (Beckman Coulter). For all subsequent experiments, [^{111}In]oxine concentrations in the tested range were used. Additional feasibility experiments using endothelial adhesion and transmigration assays under flow conditions determined that leukocytes labeled with [^{111}In]oxine remained functional (J. Allport and M.F.K., unpublished observations). Indeed, [^{111}In]oxine-labeled cells remain largely functional even 7 d after labeling (33).

Biodistribution and Autoradiography. Typically, between 0.5 and 1×10^6 cells or 50–100 μCi (1 Ci = 37 GBq) of activity, were injected i.v. into recipient mice. As control, ^{111}In alone was injected. The total amount of activity injected into each animal was measured with a radioisotope calibrator (Capintec, Ramsey, NJ). To determine blood half-life of injected monocytes, animals were bled retroorbitally every day (30 μl) until day 5. Blood samples were centrifuged and radioactivity measured in cell fractions and sera. For other experiments, at defined time points after injection, animals were anesthetized with an i.p. mixture of ketamine 100 mg/kg of body weight and xylazine 10 mg/kg of body weight. Aortas were perfused *in situ* with 3 ml of HBSS via the left ventricle. The aortas were then excised from the root to the bifurcation. All heart and fat tissue was excised to eliminate confounding signal. cpm for each aorta, kidneys, and spleen were measured by using a 1480 Wizard Wallac Gamma Counter (PerkinElmer). Percent injected dose (%ID) per g and %ID per aorta were calculated after correcting for decay, excretion, and tail radioactivity from occasional subtle extravasations. Cell number was determined by correcting for ^{111}In leakage from cells over time (free ^{111}In is rapidly excreted renally). To visualize the spatial distribution of isotope-labeled cells throughout the aorta, we used digital autoradiography with high-sensitivity screens and read-out resolutions of 50 μm (PhosphorImager screen, Molecular Dynamics).

Serum Cholesterol Measurement. At the time of killing, blood was obtained by retroorbital bleeding. Serum was obtained by centrifugation after incubating whole blood for 30 min at 37°C. Serum cholesterol levels were obtained by using a cholesterol kit (Raichem, San Diego).

ORO Staining. Excised aortas were fixed in 10% buffered formalin solution at 4°C for >10 half-lives of ^{111}In (>673 h). Aortas were then washed overnight in PBS at 4°C, pinned on silicon-elastomere in 60-mm dishes by using stainless-steel minutien pins (Fine Science Tools, Foster City, CA), washed with propylene glycol for 2 min, and placed into 0.5% ORO (Sigma) for 2–4 h at room temperature. After incubation, aortas were washed through a series of dishes containing 85% propylene glycol (Sigma) and then with PBS. Images were taken by using a digital camera and analyzed for percent lesion area by using scientific image processing program IPLAB version 3.9.4 (Scanalytics, Rockville, MD).

Data Analysis. Data are expressed as mean ± SEM. Statistical tests performed included Student's *t* test and one-way ANOVA with Tukey's multiple-comparison test. For correlation analyses, normality was tested with the Shapiro–Wilk normality test. When normality passed ($P < 0.05$), Pearson correlation was used. When normality failed ($P > 0.05$), Spearman correlation was used.

We thank Vincent Lok [Experimental Pathology Core at the Center for Molecular Imaging Research (CMIR), Massachusetts General Hospital and Harvard Medical School] and Gregory Wojtkiewicz (CMIR) for technical assistance and Timur Shtatland (CMIR) for statistical assistance. This work was supported, in part, by Grants R24 CA92782 and U01 HL080731 (to R.W.), the Donald W. Reynolds Cardiovascular Clinical Research Center on Atherosclerosis at Harvard Medical School, American Heart Association Postdoctoral Fellowships (to F.K.S. and M.F.K.), and Human Frontier Science Program Organization Grant LT00369/2003 (to M.J.P.).

1. Binder, C. J., Chang, M. K., Shaw, P. X., Miller, Y. I., Hartvigsen, K., Dewan, A. & Witztum, J. L. (2002) *Nat. Med.* **8,** 1218–1226.
2. Libby, P. (2002) *Nature* **420,** 868–874.
3. Lessner, S. M., Prado, H. L., Waller, E. K. & Galis, Z. S. (2002) *Am. J. Pathol.* **160,** 2145–2155.
4. Rajavashisth, T., Qiao, J. H., Tripathi, S., Tripathi, J., Mishra, N., Hua, M., Wang, X. P., Loussararian, A., Clinton, S., Libby, P. & Lusis, A. (1998) *J. Clin. Invest.* **101,** 2702–2710.
5. Kim, C. J., Khoo, J. C., Gillotte-Taylor, K., Li, A., Palinski, W., Glass, C. K. & Steinberg, D. (2000) *Arterioscler. Thromb. Vasc. Biol.* **20,** 1976–1982.
6. Roselaar, S. E., Kakkanathu, P. X. & Daugherty, A. (1996) *Arterioscler. Thromb. Vasc. Biol.* **16,** 1013–1018.
7. Song, L., Leung, C. & Schindler, C. (2001) *J. Clin. Invest.* **108,** 251–259.
8. Drevets, D. A., Dillon, M. J., Schawang, J. S., Van Rooijen, N., Ehrchen, J., Sunderkotter, C. & Leenen, P. J. (2004) *J. Immunol.* **172,** 4418–4424.
9. Lagasse, E. & Weissman, I. L. (1996) *J. Immunol. Methods* **197,** 139–150.
10. Sunderkotter, C., Nikolic, T., Dillon, M. J., Van Rooijen, N., Stehling, M., Drevets, D. A. & Leenen, P. J. (2004) *J. Immunol.* **172,** 4410–4417.
11. Gawaz, M., Langer, H. & May, A. E. (2005) *J. Clin. Invest.* **115,** 3378–3384.
12. Weber, C. (2005) *Circ. Res.* **96,** 612–616.
13. Groot, P. H., van Vlijmen, B. J., Benson, G. M., Hofker, M. H., Schiffelers, R., Vidgeon-Hart, M. & Havekes, L. M. (1996) *Arterioscler. Thromb. Vasc. Biol.* **16,** 926–933.
14. Zhang, S. H., Reddick, R. L., Piedrahita, J. A. & Maeda, N. (1992) *Science* **258,** 468–471.

15. Dansky, H. M., Charlton, S. A., Harper, M. M. & Smith, J. D. (1997) *Proc. Natl. Acad. Sci. USA* **94,** 4642–4646.
16. Laurat, E., Poirier, B., Tupin, E., Caligiuri, G., Hansson, G. K., Bariety, J. & Nicoletti, A. (2001) *Circulation* **104,** 197–202.
17. Muller, W. A. (2001) *J. Exp. Med.* **194,** F47–F51.
18. Patel, S. S., Thiagarajan, R., Willerson, J. T. & Yeh, E. T. (1998) *Circulation* **97,** 75–81.
19. Goldschmidt-Clermont, P. J., Creager, M. A., Lorsordo, D. W., Lam, G. K., Wassef, M. & Dzau, V. J. (2005) *Circulation* **112,** 3348–3353.
20. Buono, C., Come, C. E., Stavrakis, G., Maguire, G. F., Connelly, P. W. & Lichtman, A. H. (2003) *Arterioscler. Thromb. Vasc. Biol.* **23,** 454–460.
21. Frostegard, J., Ulfgren, A. K., Nyberg, P., Hedin, U., Swedenborg, J., Andersson, U. & Hansson, G. K. (1999) *Atherosclerosis* **145,** 33–43.
22. Boring, L., Gosling, J., Cleary, M. & Charo, I. F. (1998) *Nature* **394,** 894–897.
23. Reckless, J., Rubin, E. M., Verstuyft, J. B., Metcalfe, J. C. & Grainger, D. J. (1999) *Circulation* **99,** 2310–2316.
24. Nakashima, Y., Raines, E. W., Plump, A. S., Breslow, J. L. & Ross, R. (1998) *Arterioscler. Thromb. Vasc. Biol.* **18,** 842–851.
25. Sukhova, G. K., Zhang, Y., Pan, J. H., Wada, Y., Yamamoto, T., Naito, M., Kodama, T., Tsimikas, S., Witztum, J. L., Lu, M. L., *et al.* (2003) *J. Clin. Invest.* **111,** 897–906.
26. Buono, C., Pang, H., Uchida, Y., Libby, P., Sharpe, A. H. & Lichtman, A. H. (2004) *Circulation* **109,** 2009–2015.
27. Mach, F., Schonbeck, U., Sukhova, G. K., Atkinson, E. & Libby, P. (1998) *Nature* **394,** 200–203.
28. Hajra, L., Evans, A. I., Chen, M., Hyduk, S. J., Collins, T. & Cybulsky, M. I. (2000) *Proc. Natl. Acad. Sci. USA* **97,** 9052–9057.
29. Eriksson, E. E., Xie, X., Werr, J., Thoren, P. & Lindbom, L. (2001) *J. Exp. Med.* **194,** 205–218.
30. Eriksson, E. E., Xie, X., Werr, J., Thoren, P. & Lindbom, L. (2001) *FASEB J.* **15,** 1149–1157.
31. Steinberg, D., Khoo, J. C., Glass, C. K., Palinski, W. & Almazan, F. (1997) *Proc. Natl. Acad. Sci. USA* **94,** 4040–4044.
32. Llodra, J., Angeli, V., Liu, J., Trogan, E., Fisher, E. A. & Randolph, G. J. (2004) *Proc. Natl. Acad. Sci. USA* **101,** 11779–11784.
33. Kraitchman, D. L., Tatsumi, M., Gilson, W. D., Ishimori, T., Kedziorek, D., Walczak, P., Segars, W. P., Chen, H. H., Fritzges, D., Izbudak, I., *et al.* (2005) *Circulation* **112,** 1451–1461.